01 Jul 2020

A Feasible Approach To Predicting Time-dependent Bearing Performance Of Jacked Piles From CPTu Measurements

Lin Li

Jingpei Li

De'an Sun

Weibing Gong
Missouri University of Science and Technology, weibing.gong@mst.edu

Recommended Citation

L. Li et al., "A Feasible Approach To Predicting Time-dependent Bearing Performance Of Jacked Piles From CPTu Measurements," *Acta Geotechnica*, vol. 15, no. 7, pp. 1935 - 1952, Springer, Jul 2020.
The definitive version is available at https://doi.org/10.1007/s11440-019-00875-x

Acta Geotechnica (2020) 15:1935–1952
https://doi.org/10.1007/s11440-019-00875-x

RESEARCH PAPER

A feasible approach to predicting time-dependent bearing performance of jacked piles from CPTu measurements

Lin Li[1] · Jingpei Li[1] · De'an Sun[2] · Weibing Gong[1]

Received: 31 December 2018 / Accepted: 29 September 2019 / Published online: 16 November 2019

Abstract

In this paper, a simple but feasible approach is proposed to predict the time-dependent load carrying behaviours of jacked piles from CPTu measurements. The corrected cone resistance, which considers the unequal area of the cone rod and the cone, is used to determine the soil parameters used in the proposed approach. The pile installation effects on the changes in the stress state of the surrounding soil are assessed by an analytical solution to undrained expansion of a cylindrical cavity in K_0-consolidated anisotropic clayey soil. Considering the similarity and scale effects between the piezocone and the pile, the CPTu measurements are properly incorporated in the shaft and end resistance factors as well as in the load-transfer curves to predict the time-dependent load carrying behaviours of the pile. Centrifuge model tests are conducted and the measured load carrying behaviours of the model piles are compared with the predictions to validate the proposed approach. The proposed approach not only greatly saves the time of conducting time-consuming pile load tests, but also effectively avoids solving the complex partial differential equations involved in the consolidation analysis, and hence is feasible enough to determine the time-dependent load carrying behaviours of jacked piles in clay.

Keywords Centrifuge model test · Corrected cone resistance · CPTu measurements · Load carrying behaviours · Time-dependent

List of symbols

A, B	Parameters for simplifying expression
A_1, A_2	Cross-sectional areas of the cone rod and cone shaft
A_p	Cross-sectional area of pile
$A_{s,i}$	Area of pile shaft in soil layer i
a	Net area ratio
$a_b(t), a_{s,z}(t)$	Time-dependent model parameters of the load-transfer curve for pile toe and shaft, respectively
$b_b(t), b_{s,z}(t)$	Time-dependent model parameters of the load-transfer curve for pile toe and shaft, respectively
$C_q(t)$	Time-dependent pile toe resistance factor
c_h	Horizontal consolidation coefficient
D_{pile}, D_{CPTu}	Diameters of pile and piezocone
e	Void ratio
$F_{su}(t), F_{qu}(t)$	Time-dependent pile shaft bearing capacity and pile toe capacity
f_s	Sleeve friction
f_{su}	Ultimate shaft resistance
$f_{su,i}(t)$	Time-dependent ultimate shaft resistance in layer i
$f_{su,z}(t)$	Time-dependent ultimate shaft resistance at depth z
G	Shear modulus
G_0	In situ shear modulus
K_0	Coefficient of earth pressure at rest
$K_{0,b}(t)$	Time-dependent initial stiffness of pile toe

✉ Jingpei Li
lijp2773@tongji.edu.cn

Lin Li
lilin_sanmao@163.com

De'an Sun
sundean@shu.edu.cn

Weibing Gong
weibingthomas@163.com

[1] Department of Geotechnical Engineering, Tongji University, Shanghai 200092, China

[2] Department of Civil Engineering, Shanghai University, Shanghai 200444, China

$K_{0,z}(t)$	Time-dependent initial stiffness of the soil column with unit length at the pile–soil interface
k_h	Horizontal coefficient of permeability
L	Length of pile
M	Slope of critical state line
N_c	Pile toe resistance factor
N_{ke}	Cone resistance factor
OCR	Overconsolidation ratio
p'_0	Far-field geostatic mean effective stress
$p'(t)$	Mean effective stress of the soil adjacent to the pile shaft during consolidation
p'_f	Mean effective stress of soil in the vicinity of the pile immediately after pile installation
$Q_u(t)$	Time-dependent total load carrying capacity
$q_b(t)$	Mobilized resistance at pile toe
q_{bu}	Ultimate pile toe resistance
$q_{bu}(t)$	Pile toe resistance at any time after pile installation
q_c	Cone tip resistance
q_e	Effective cone tip resistance
$\bar{q}_e$	Average effective cone resistance in pile toe influence zone
q_t	Corrected cone tip resistance
R_f	Failure ratio
r	Radial distance from pile axis
r_m	Limiting radius beyond which shear stress induced by pile loading is negligible
r_p	Pile radius
γ_w	Unit weight of water
r_y	Radius of plastic zone developed around pile
$s_{u,tc}, s_{u,ps}$	Undrained shear strengths of soil under triaxial compression condition and plane strain condition, respectively
T	Non-dimensional time
T_{pile}, T_{CPTu}	Non-dimensional time for dissipation of normalized excess pore pressure around the pile and piezocone, respectively
t_{pile}, t_{CPTu}	Real consolidation time of the soil around the pile and piezocone
$U_{pile}(t), U_{pile}(t)$	Degrees of consolidation of the soil around the pile and piezocone
u	Pore water pressure
u_1, u_2, u_3	Measured pore water pressures at cone tip, shoulder and shaft
v'	Effective Poisson's ratio
W_b	Displacement at pile toe
$W_{s,z}$	Pile–soil relative displacement at depth z
α	Shaft resistance factor of total stress method
$\alpha_c(t)$	Time-dependent shaft resistance factor
β	Shaft resistance factor of effective stress method
Δu	Excess pore water pressure
$\Delta u_{pile}, \Delta u_{CPTu}$	Excess pore water pressure around the pile and the piezocone
Δu_t	Limit excess pore water pressure developed at the wall of an expanding spherical cavity
η_0	Initial stress ratio of soil
η^*_y	Relative stress ratio at the elastic–plastic boundary
κ	Slope of swelling line in e-ln p' plane
Λ	Plastic volumetric strain ratio
λ	Slope of compression line in e-ln p' plane
υ	Specific volume
ξ	Parameter for simplifying expression
ρ_s	Ratio of undrained shear strength at any given time after installation to in situ undrained shear strength
ρ_G	Ratio of shear modulus at any given time after installation to in situ shear modulus
σ'_r, σ'_z	Radial and vertical effective stresses
σ_u	Limit expansion pressure
σ'_{v0}	Effective vertical stress
$\sigma'_{rf}, \sigma'_{zf}$	Radial and vertical effective stresses at failure
τ_{rzf}	Shear stress at failure
$\tau_{s,z}(t)$	Mobilized shaft shear resistance
φ'	Internal effective friction angle of soil
χ	Ratio of soil shear modulus at middle depth to that of the pile toe
ψ_f	Stress-transformed parameter under plane strain condition

1 Introduction

Installation of a jacked pile in clay inevitably causes severe squeezing and shearing effects on the surrounding soils, which not only changes the original state of the soil but also generates larger excess pore water pressures in the vicinity of the pile. After installation, the disturbed/remoulded soil recovers its strength with dissipation of the generated excess pore water pressure. As a consequence, the load carrying capacity of the pile increases with time

and exhibits apparently time-dependent loading carrying behaviour (referred to as "setup effect"). In pile design and construction, underestimation of setup might result in unnecessary costs, while overestimation would bring great peril to the upper structure supported by the piles as the pile capacity never reaches its design value [18]. However, because of the extremely complex changes in mechanical properties of the surrounding soil during installation and subsequent consolidation, the setup effects are occasionally ignored in the current jacked pile design [6], although the significance of setup has been widely addressed in the past few decades (e.g. [2, 4, 6, 27, 28, 33, 56, 58, 70].

Currently, numerous methods are available for determining the pile load carrying capacity. These methods can be broadly classified into four categories: (1) total stress methods (α method); (2) effective stress methods (β method); (3) cone penetration test (CPT)/piezocone penetration test (CPTu) methods; and (4) in situ/laboratory pile loading tests. The total stress methods and the effective methods are the two most commonly used approaches in the pile design because of their simplicity [20]. However, because the total stress methods and the effective stress methods directly correlate the pile shaft and toe resistances to the in situ undrained shear strength or effective stress of surrounding soil through the empirical factor α or β, they are incapable of properly considering the complex stress–strain changes occurring during pile installation, equalization and loading. As a result, they yield poor predictive reliability when directly applied in the jacked pile design [15, 29]. Moreover, the in situ soil properties used in the total stress methods and the effective methods are hard to be accurately determined from laboratory tests, which makes the two methods less desirable than the CPTu methods. Although the pile loading test, especially the in situ test, is considered as the most reliable approach in determining the pile load carrying capacity, it is prohibitively expensive and time-consuming to conduct pile load tests when the time-dependent behaviours are involved [8, 53]. Compared with other methods, the CPT/CPTu methods are robust, simple and reliable in predicting pile load carrying capacity as the CPT/CPTu methods directly or indirectly correlate the measurements to the pile load carrying capacity, which effectively avoids the uncertainties in determining intermediate parameters from the conventional laboratory tests [11, 21, 42, 45].

As commonly reported, the direct method and indirect method are the two main CPT/CPTu approaches for pile capacity evaluation [11, 45]. In the direct methods, the CPT/CPTu is considered as a mini-pile, based on which the cone tip resistance and the sleeve friction are directly scaled up or down via correlation factors to predict the pile shaft and toe resistances. Since the correlation factors used in the direct method are obtained from statistical analysis of the relations between the CPT/CPTu profiles and the corresponding pile load test results [11, 21], the predictive performance of the direct CPT/CPTu method greatly depends on the database utilized. Up to now, extensive research efforts have been dedicated to calibrating the correlation factors with different databases to improve the predictive performance of the direct CPT/CPTu methods (e.g. [1, 11, 14, 21, 22, 25, 42, 43, 46, 55, 57, 69, 72]. These efforts have definitely improved the performance of the direct CPT/CPTu methods. However, these proposed correlation factors still need further calibration before they are applied to other different soil conditions as they are developed from specific regions and geologies. Moreover, since the correlation factors are deduced from the pile load tests at a certain time after pile installation, the setup effects of the pile are still left unconsidered in the direct approaches. Different from the direct methods, the indirect CPT/CPTu methods first deduce the basic soil parameters, such as the overconsolidation ratio, the undrained shear strength, the effective stress, the lateral pressure coefficient and internal friction angle, from CPT/CPTu measurements. These parameters are then used as the inputs to evaluate the load carrying capacity of the pile utilizing either empirical or theoretical formulas [19]. Compared with the direct methods, the indirect CPT/CPTu methods consider the specific soil properties and hence are applicable to different soil conditions. However, although the CPTu can record the excess pore water pressure during sounding and the corresponding dissipation process, the pore pressure data are rarely applied to predict the setup effects of jacked piles in clay. The rational approaches to predicting the setup and long-term load carrying behaviour of jacked piles from CPTu measurements are still not currently available.

This paper presents a rational and feasible CPTu method to predict the time-dependent load carrying behaviours of jacked piles in clay. The soil properties used in the proposed approach are extracted from the corrected cone resistance. The pile installation effects are evaluated by an analytical solution to undrained expansion of a cylindrical cavity in K_0-consolidated anisotropic soil. The proposed approach, which properly incorporates the installation effects and makes use of the CPTu measurements, is then developed based on the similarity of the piezocone and the pile to predict the time-dependent load carrying capacity and load–displacement behaviours of jacked piles in clay. The proposed framework is validated by comparing the predictions with the measured results from centrifuge model tests conducted by the authors at Tongji University. The proposed approach not only reasonably makes use of the CPTu measurements, but also considers the pile installation effects, the scale effects, the three-dimensional strength and the stress anisotropy of the soil, and thus is capable of yielding reasonable predictions for the time-

dependent load carrying behaviours of jacked piles. It is expected that the proposed approach could serve as a feasible tool to incorporate the setup effects in the jacked pile design.

2 Measured data from CPTu and determination of soil parameters

2.1 CPTu measurements and penetration model

CPTu is an efficient way of inferring in situ geotechnical parameters. In the penetration process, the piezocone can continuously measure and record the cone tip resistance, q_c, the sleeve friction, f_s, and the pore water pressure, u, at the position of pore pressure transducer. Currently, the position of the pore pressure transducer has not been standardized for piezocone [39, 59]. As shown in Fig. 1, the pore pressure filter can be placed either on the cone face, or behind the cone shoulder or behind the friction sleeve. For the piezocone with pore pressure filter at the shoulder position, the measured cone tip resistance should be corrected with the pore water pressure due to the unequal area of the cone rod and the cone, as shown in Fig. 2. In this study, the proposed framework is developed based on the piezocone with pore pressure filter behind the cone shoulder and hence the unit cone tip resistance should be firstly corrected with the pore water pressure at the cone shoulder before it is used in soil classification [35, 40]

$$q_t = q_c + (1 - a)u_2 \tag{1}$$

where q_t is the corrected cone resistance; a $(= A_1/A_2)$ is the net area ratio; A_1 and A_2 are the cross-sectional areas of

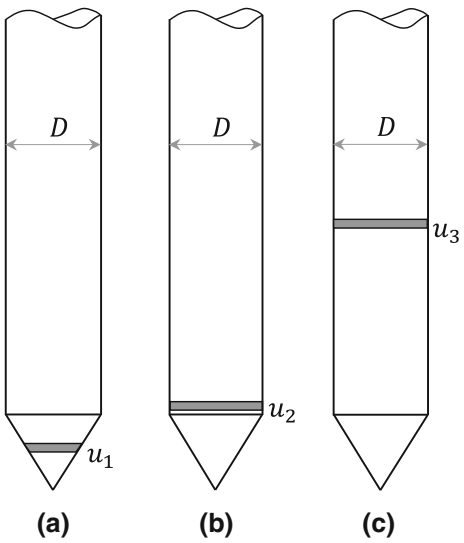

Fig. 1 Different locations of pore pressure transducer: **a** at cone face; **b** behind cone shoulder; **c** behind friction sleeve

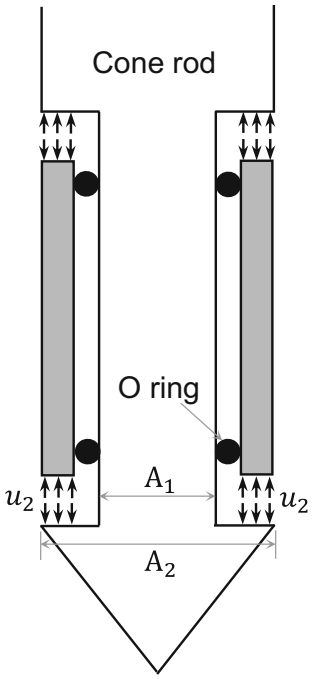

Fig. 2 Schematic of unequal end area of piezocone

the and the cone rod and cone shaft, respectively; and u_2 is the measured pore water pressure at the cone shoulder. For a typical piezocone, the value of the net area ratio can be usually taken as 0.8 in most cases.

Up to date, many approaches have been developed to interpret cone penetration tests, and these approaches mainly include: cavity expansion theory [9, 13, 63, 71], strain path method [5] and finite-element method [26, 61, 62]. Among these approaches, the cavity expansion theory has been the most popular approach utilized in interpretation cone penetration tests, because not only the displacement field developed around an expanding spherical cavity resembles that around the cone tip, but also the soil properties, such as the undrained shear strength, the rigidity, the overconsolidation ratio and the stress state of the soil could be properly considered in the simple closed-form solution [13, 71]. Hence, the solution to an undrained expansion of a spherical cavity in modified Cam-clay soils proposed by Cao et al. [12] is employed in this study to model the piezocone penetration test. Following Cao et al. [12], the limit expansion pressure, σ_u, and the limit excess pore water pressure, Δu_t, developed at the wall of an expanding spherical cavity can be given as

$$\sigma_u = \frac{4}{3} s_{u,tc} \left(\ln \frac{G}{s_{u,tc}} + 1 \right) + p_0' \tag{2}$$

$$\Delta u_t = \frac{4}{3} s_{u,tc} \ln \left(\frac{G}{s_{u,tc}} \right) + p_0' \left[1 - \left(\frac{OCR}{2} \right)^{\Lambda} \right] \tag{3}$$

where G is the shear modulus; OCR is the overconsolidation ratio; $\Lambda = 1 - \kappa/\lambda$ is the plastic volumetric strain ratio, the value of which falls in the range of 0.7–0.8 for wide range of clays; p'_0 is the far-field geostatic mean effective stress; λ and κ are the slopes of compression and swelling lines in the e-ln p' plane, respectively; and $s_{u,tc}$ is the undrained shear strength of soil under the triaxial compression condition. In the critical state soil mechanics, the shear modulus G and undrained shear strength $s_{u,tc}$ are defined as [68]

$$G = \frac{3(1-2\nu')\upsilon p'_0}{2(1+\nu')\kappa} \tag{4}$$

$$s_{u,tc} = \frac{1}{2} M p'_0 \left(\frac{\mathrm{OCR}}{2}\right)^{\Lambda} \tag{5}$$

where ν' is the effective Poisson's ratio; υ is the specific volume; and $M = 6\sin\varphi'/(3-\sin\varphi')$ is the slope of critical state line; here, φ' is the internal effective friction angle of soil.

Equation (3) in fact is similar to the solution for the limit excess pore pressure proposed by Burns and Mayne [10] in the interpretation of piezocone test. The only difference is that the mean effective pressure p'_0 rather than the effective vertical stress σ'_{v0} is utilized in Eq. (3). Since both the strength and shear modulus depend on the mean effective stress of the soil, Eq. (3) could yield more reasonable excess pore pressure when it is applied in interpretation of piezocone test. As indicated by Burns and Mayne [10], the first term on the right-hand side of Eq. (3) represents the excess pore pressure induced by the changes in the octahedral normal stress of the soil, while the second term represents the excess pore water pressure resulting from the change in the octahedral shear stress.

2.2 Determination of soil parameters

Theoretically, the cone tip resistance is composed of the vertical components of limit expansion pressure and the shear resistance of the soil along the cone surface, as shown in Fig. 3. Based on the limit expansion pressure σ_u given in Eq. (2), the corrected tip resistance can be derived from the equilibrium condition in the vertical direction as follows:

$$q_t = \frac{4}{3} s_{u,tc}\left(\ln\frac{G}{s_{u,tc}} + 1\right) + p'_0 + \sqrt{3}s_{u,tc} \tag{6}$$

Combining Eq. (3) with Eq. (6), the overconsolidation ratio of the soil, one of the significant soil parameters affecting the soil behaviour, can be determined as

$$\mathrm{OCR} = 2\left[\frac{q_e}{p'_0(1+1.53M)}\right]^{1/\Lambda} \tag{7}$$

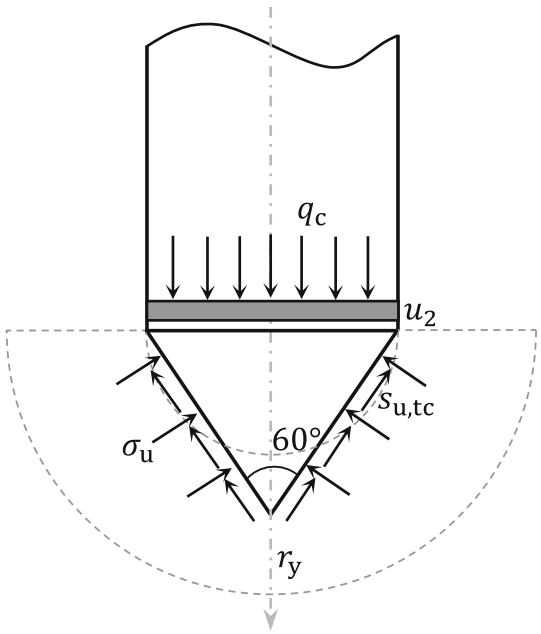

Fig. 3 Theoretical model for cone penetration and stress distribution at cone tip

where $q_e = q_t - u_1$ is the effective cone tip resistance and u_1 is the pore water pressure at the cone tip, the value of which is generally larger than the measured pore water pressure u_2 at the cone shoulder. In most cases, u_1 is in the order of $(1 \sim 1.1)$ times u_2 [54].

Since the strain field developed around the cone tip resembles that around an expanding spherical cavity, the two tangential stresses around the cone tip are equal to each other, the stress state of which is similar to that under triaxial compression state. Hence, substituting Eq. (7) into Eq. (5), the in situ undrained shear strength in terms of triaxial compression can be related to the effective cone resistance as follows:

$$s_{u,tc} = \frac{q_e}{N_{ke}} \tag{8}$$

where $N_{ke} = 2(1+1.53M)/M$ is defined as the cone resistance factor.

It should be mentioned here that since the proposed approach is developed based on the CPTu measurements, the in situ shear modulus of the soil used in the proposed approach still needs to be additionally determined from the laboratory test. Hence, the seismic piezocone tests (SCPTu) seems more suitable and should be considered in future study for predicting the time-dependent bearing performance of jacked piles, as both the shear strength and the shear modulus of the soil could be determined from the SCPTu measurements.

3 Mechanical properties of soil around jacked piles

3.1 Pile installation effects

Installation of a jacked pile generally causes significant compression effects on the surrounding soil, which changes the initial stress state of the soil and generates a large amount of excess pore water pressure to accommodate the squeezing effects. Appropriate assessment of the pile installation effect is crucial for determining the time-dependent load carrying behaviour of the pile after installation. Since the deformation mechanism of the soil around the pile shaft is similar to the expansion of a cylindrical cavity, the pile installation effects on the surrounding soils could be properly assessed by the cylindrical cavity expansion theory [23, 47, 51, 74]. Given the fact that the initial stress state of most natural clay deposits is anisotropic due to their deposition and K_0 consolidation [17, 60, 67], the elasto-plastic solution for cylindrical cavity expansion, presented by Li et al. [32] based on an anisotropic modified Cam-clay (AMCC) model, is employed in this study to evaluate the pile installation effects. Taking pile installation as undrained expansion of a cylindrical cavity from zero initial radius to the pile radius, the excess pore water pressure, Δu_{pile}, induced by pile installation and the mean effective stress of the soil, p'_{f}, in the vicinity of the pile immediately after pile installation can be approximately evaluated by the cavity expansion solution of Li et al. [32], respectively, as follows:

$$\Delta u_{\text{pile}} = p'_0\left[\frac{3K_0}{2K_0+1}+\frac{1}{\sqrt{3}}\eta^*_{\text{y}}-\left(\frac{\text{OCR}}{2}\right)^{\Lambda}\right] + p'_{\text{f}}\left(\xi\ln\frac{r_{\text{y}}}{r}-\frac{1}{2}\xi\pm\frac{\sqrt{4M^2-3\xi^2}}{6}\right) \tag{9}$$

$$p'_{\text{f}} = p'_0\left(\frac{\text{OCR}}{2}\right)^{\Lambda} \tag{10}$$

where K_0 is the coefficient of earth pressure at rest. If $K_0 \geq 1$, Eq. (9) adopts the minus sign in the last bracket; on the contrary, the minus should be used if $K_0 < 1$. ξ is a parameter used for simplifying the equation expression; r_{y} is the radius of plastic zone developed around the pile; r is the radial distance from pile axis; and η^*_{y} is the relative stress ratio at the elastic–plastic boundary. The expressions of ξ, η^*_{y}, r_{y} and q_{f} are given as follows:

$$\xi = \frac{2\sqrt{3\left[M^2(2K_0+1)^2-9(K_0-1)^2\right]}}{3(2K_0+1)} \tag{11}$$

$$\frac{r_{\text{y}}}{r_{\text{p}}} = \sqrt{\frac{\sqrt{3}G_0}{p'_0\eta^*_{\text{y}}}} \tag{12}$$

$$\eta^*_{\text{y}} = \sqrt{(\text{OCR}-1)\left(M^2-\eta_0^2\right)} \tag{13}$$

where $\eta_0 = |3(1-K_0)/(2K_0+1)|$ is the initial stress ratio of the soil; r_{p} is the radius of the pile; and $G_0 = 3(1-2\nu')\upsilon p'_0/\left[2\left(1+\nu'\right)\kappa\right]$ is the in situ shear modulus.

3.2 Consolidation of soil after pile installation

After pile installation, the disturbed soil reconsolidates with dissipation of the excess pore water pressure generated by installation. As a result, the effective stress of the soil adjacent to the pile increases with the elapse of time, which is the primary cause for the time-dependent load carrying behaviours of a jacked pile in clay [6]. Theoretically, the consolidation phase can be analysed based on either the Terzaghi's consolidation theory or the Biot's coupled consolidation theory. However, the stiffness difference in the soil around the pile caused by pile installation, which would result in significant relaxation in the total stress during consolidation, is hard to be incorporated in the consolidation analysis [47]. Hence, it is nearly impossible or extremely complex to obtain an appropriate analytical solution to evaluate the dissipation of the excess pore water pressure.

Given the fact that the geometry and the penetration process of piezocone are similar to those of a jacked pile, the relaxation effects and the dissipation of the excess pore water pressure could be reasonably assessed from the piezocone dissipation tests. As shown by Randolph [47], the dissipation curves for piles with different diameters nearly overlap each other if the curves are presented in terms of the normalized excess pore pressure, $\Delta u(T)/\Delta u(T=0)$, and the non-dimensional time, $T\left(=c_{\text{h}}t/D^2_{\text{pile}}\right)$, where $\Delta u(T)$ and $\Delta u(T=0)$ denote the excess pore water pressure at any time after installation and immediately after pile installation, respectively; D_{pile} is the pile diameter; $c_{\text{h}}(=k_{\text{h}}G/\gamma_{\text{w}})$ is the horizontal consolidation coefficient; k_{h} is the horizontal coefficient of permeability; and γ_{w} is the unit weight of water. Here, the horizontal consolidation and permeability coefficients are employed because both the field test and theoretical studies show that the excess pore water pressure around the pile shaft vanishes predominately in the radial direction [23, 53].

Based on the above observation of Randolph [47], it can be concluded that the non-dimensional time required for dissipation of certain amount of normalized excess pore pressure around the pile, T_{pile}, is equal to the non-dimensional time required for dissipation of the same amount of

normalized excess pore pressure around the piezocone, T_{CPTu}, i.e.

$$T_{\mathrm{pile}} = T_{\mathrm{CPTu}} \tag{14}$$

According to the definition of the non-dimensional time, the real consolidation time of the soil around the pile, t_{pile}, can be expressed by the real consolidation time of the soil around the piezocone, t_{CPTu}, as

$$t_{\mathrm{pile}} = \frac{D_{\mathrm{pile}}^2}{D_{\mathrm{CPTu}}^2} t_{\mathrm{CPTu}} \tag{15}$$

where D_{CPTu} is the diameter of the piezocone.

Utilizing Eq. (15), the degree of consolidation of the soil around the pile, $U_{\mathrm{pile}}(t)$, defined as the percentage excess pore water pressure dissipated at any time to the initial excess pore water pressure to be dissipated, can be evaluated through the excess pore water pressure measured from the piezocone dissipation test as follows:

$$U_{\mathrm{pile}}(t) = 1 - \frac{\Delta u_{\mathrm{pile}}(t)}{\Delta u_{\mathrm{pile}}(t=0)} = 1 - \frac{\Delta u_{\mathrm{CPTu}}\left(D_{\mathrm{pile}}^2 t / D_{\mathrm{CPTu}}^2\right)}{\Delta u_{\mathrm{CPTu}}(t=0)} \tag{16}$$

where Δu_{pile} and Δu_{CPTu} are the excess pore water pressure around the pile and the piezocone, respectively.

Equation (16) indicates that the consolidation rate is inversely proportional to the square of the pile diameter. For a typical piezocone with a diameter of 36 mm, the time required for full consolidation of the surrounding soil is only one percentage of the time required for full consolidation of the soil around a pile with a diameter of 36 cm. Indeed, many in situ tests have shown that the excess pore water pressure around the piezocone fully dissipates just in several hours (e.g. [3, 10, 52], while the dissipation of the excess pore water pressure around the pile lasts for several weeks or even several months [53]. Hence, the dissipation data from piezocone provide a quick and feasible estimation for the consolidation of the soil around the pile, which not only greatly reduces the time required to conduct pile load test after full dissipation of the excess pore water pressure, but also avoids solving the complex governing equations involved in consolidation analysis.

After pile installation, the soil around the pile consolidates approximately under a plane strain condition and the mean effective stress, $p'(t)$, of the soil adjacent to the pile shaft during consolidation can be approximately given as [49]

$$p'(t) = p'_{\mathrm{f}} + \frac{1+\nu'}{3(1-\nu')}\left[\Delta u_{\mathrm{pile}}(t=0) - \Delta u_{\mathrm{pile}}(t)\right] \tag{17}$$

Combining Eqs. (15) and (17), the mean effective stress $p'(t)$ can be related to the excess pore pressure measurement from the CPTu as follows:

$$p'(t) = p'_{\mathrm{f}} + \frac{1+\nu'}{3(1-\nu')}\left[1 - \frac{\Delta u_{\mathrm{CPTu}}\left(D_{\mathrm{pile}}^2 t / D_{\mathrm{CPTu}}^2\right)}{\Delta u_{\mathrm{CPTu}}(t=0)}\right] \Delta u_{\mathrm{pile}}(t=0) \tag{18}$$

Since both the undrained shear strength and the shear modulus, two key parameters governing the pile behaviour, depend on the mean effective stress of the soil, Eqs. (17) and (18) could be further utilized to assess the time-dependent load carrying behaviours of the pile, which is the major task in the following sections.

3.3 Soil properties after installation

The severe squeezing effect induced by pile installation not only changes the stress state of the surrounding soil, but also disrupts the preconsolidation stress history of the soil around the pile, especially the soil in the vicinity of the pile. Hence, after pile installation, the soil adjacent to the pile can be approximately taken as the normally consolidated soil with OCR = 1 [50]. Based on this approximation and Eq. (5), the undrained shear strength of the soil adjacent to the pile at any time after installation, $s_{\mathrm{u,tc}}\left(r_{\mathrm{p}}, t\right)$, can be given as

$$s_{\mathrm{u,tc}}\left(r_{\mathrm{p}}, t\right) = \frac{1}{2} M p'(t) \left(\frac{1}{2}\right)^{\Lambda} \tag{19}$$

The shear modulus, as shown in Eq. (4), also depends on the mean effective stress. Hence, the shear modulus of the soil adjacent to the pile at any time after installation can be given as

$$G\left(r_{\mathrm{p}}, t\right) = \frac{3(1-2\nu')\upsilon p'(t)}{2(1+\nu')\kappa} \tag{20}$$

Based on Eqs. (5), (16), (17) and (19), the shear strength ratio, $\rho_{\mathrm{s}}(t)$, defined as the ratio of the undrained shear strength at any given time after installation to the in situ undrained shear strength, can be expressed as

$$\rho_{\mathrm{s}}(t) = \frac{s_{\mathrm{u,tc}}\left(r_{\mathrm{p}}, t\right)}{s_{\mathrm{u,tc}}} = \left(\frac{1}{2}\right)^{\Lambda} + \frac{1+\nu'}{3(1-\nu')} \frac{\Delta u_{\mathrm{pile}}(t=0)}{p'_0(\mathrm{OCR})^{\Lambda}} U_{\mathrm{pile}}(t) \tag{21}$$

Similarly, based on Eqs. (4), (16), (17) and (20), the shear modulus ratio, $\rho_{\mathrm{G}}(t)$, defined as the ratio of the shear modulus at any given time after installation to the in situ shear modulus G_0, can be given as

$$\rho_{\mathrm{G}}(t) = \frac{G\left(r_{\mathrm{p}}, t\right)}{G_0} = \left(\frac{\mathrm{OCR}}{2}\right)^{\Lambda} + \frac{1+\nu'}{3(1-\nu')} \frac{\Delta u_{\mathrm{pile}}(t=0)}{p'_0} U_{\mathrm{pile}}(t) \tag{22}$$

It should be noted that both consolidation and soil ageing would result in the setup of jacked piles after pile installation. Nevertheless, the setup is primarily attributable to the increase in effective stress due to soil consolidation, while soil ageing that refers to a time-dependent change in soil properties at a constant effective stress contributes little to pile setup compared with the setup caused by consolidation. Hence, soil ageing, which is beyond the scope of this study, is not considered in the proposed approach.

4 Prediction of time-dependent load carrying capacity

4.1 Pile shaft resistance

As shown in Fig. 4, the soil around the pile deforms in the vertical annular plane without radial deformation during pile loading, which is similar to the deformation under the plane strain condition. Hence, the shear strength of the soil around the pile can be approximately evaluated from the shear strength measured in the simple shear test that is under plane strain condition [50]. Since the soil exhibits different strengths under different loading conditions [37], the undrained strength determined from the cone tip resistance by Eq. (8) in terms of triaxial condition should be transformed to the shear strength under the plane strain condition in order to predict the shaft resistance. In this study, the spatially mobilized plane (SMP) criterion proposed by Matsuoka [36], which appropriately considers effect of intermediate principal stress and hence is capable of reflecting the three-dimensional strength of the soil under various loading conditions, is employed to model the shear strength of the soil adjacent to the pile that deforms approximately under plane strain condition. Following Matsuoka et al. [38], the undrained shear strength under plane strain condition, $s_{u,ps}$, can be deduced from the undrained shear strength under triaxial condition as follows:

$$s_{u,ps} = \frac{3\sin\psi_f}{M\sqrt{2+\sin^2\psi_f}} s_{u,tc} \tag{23}$$

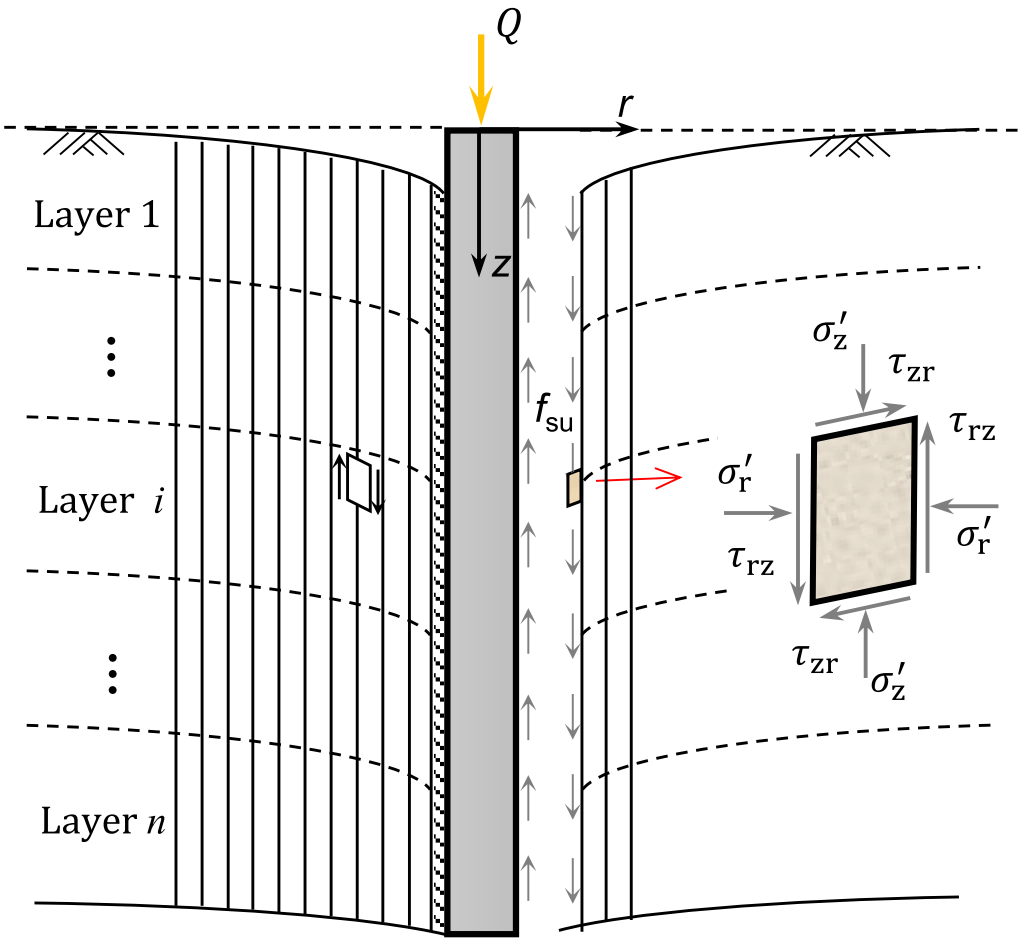

Fig. 4 Deformation of soil surrounding pile and stress states of a soil element adjacent to pile shaft during loading

where $\psi_f = \arcsin\left(\sqrt{2}M/\sqrt{9+3M}\right)$ is the stress-transformed parameter under plane strain condition.

Following Randolph and Wroth [50], the failure stress state of a soil element adjacent to the pile shaft during pile loading can be plotted in the $\sigma' - \tau$ plane, as shown in Fig. 5. In Fig. 5, the failure envelope passes through the original of the coordinates since the soil after installation could be taken as the normally consolidated soil. Due to the severe squeezing effect caused by pile installation, the radial effective stress σ'_r of the soil element adjacent to the pile shaft is larger than the vertical effective stress σ'_z after installation. Hence, the failure envelope is tangent to the Mohr's stress circle at point $F(\sigma'_{zf}, \tau_{zrf})$ when the soil reaches failure state [50]. The ultimate shaft resistance, f_{su}, which is equal to the failure shear stress, τ_{rzf}, could be deduced from the geometrical relationship in Fig. 5 as follows:

$$f_{su} = \tau_{rzf} = s_{u,ps}\cos\varphi' \tag{24}$$

Combining Eqs. (8), (19), (21), (23) and (24), the shaft resistance, $f_{su}(t)$, at any time after installation could be related to the effective cone tip resistance as follows:

$$f_{su}(t) = \alpha_c(t) q_e \tag{25}$$

where $\alpha_c(t)$ is defined as the shaft resistance factor based on CPTu data, which can be expressed as

$$\alpha_c(t) = \frac{3\rho_s(t)\sin\psi_f\cos\varphi'}{N_{KE}M\sqrt{2+\sin^2\psi_f}} \tag{26}$$

It can be seen from Eq. (26) that the time-dependent pile shaft resistance factor $\alpha_c(t)$ is proportion to the degree of consolidation and hence can be expressed by the degree of consolidation as

$$\alpha_c(t) = \alpha_c(t=0) + [\alpha_c(t=\infty) - \alpha_c(t=0)]U_{pile}(t) \tag{27}$$

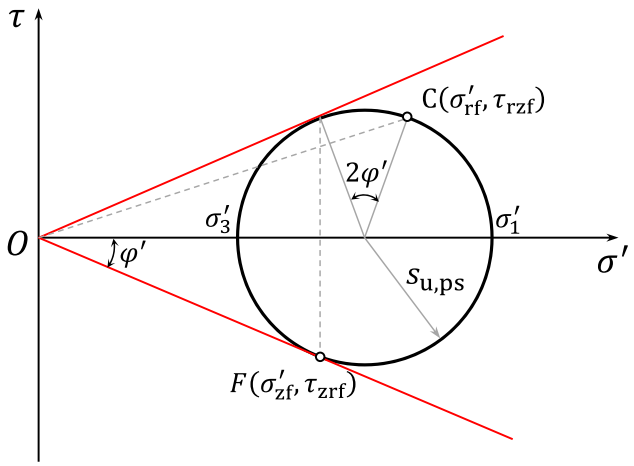

Fig. 5 Failure stress state of soil element adjacent to pile shaft in $\sigma' - \tau$ plane

Based on Eqs. (16) and (27), the time-dependent pile shaft resistance factor $\alpha_c(t)$ can be further related to the dissipation data from piezocone as follows:

$$\alpha_c(t) = \alpha_c(t=0) + [\alpha_c(t=\infty) - \alpha_c(t=0)]\left[1 - \frac{\Delta u_{CPTu}\left(D^2_{pile}t/D^2_{CPTu}\right)}{\Delta u_{CPTu}(t=0)}\right] \tag{28}$$

where $\alpha_c(t=0)$ corresponds to the shaft resistance factor immediately after installation and $\alpha_c(t=\infty)$ denotes the long-term shaft resistance factor.

4.2 Pile toe resistance

For jacked piles in clayey soils, the ultimate pile toe resistance can be simply estimated as [64]

$$q_{bu} = N_c s_{u,tc} \tag{29}$$

where N_c is the pile toe resistance factor, the value of which is in the order of 9 for a wide range of clayey soils [7, 66].

Combining Eqs. (8), (21), and (29), the ultimate pile toe resistance at any time after installation, $q_{bu}(t)$, can be expressed as follows:

$$q_{bu}(t) = \rho_s(t)N_c/N_{ke} = C_q(t)\bar{q}_e \tag{30}$$

where $C_q(t)$ $(= \rho_s(t)N_c/N_{ke})$ is defined as the pile toe resistance factor based on CPTu data. Note that $C_q(t)$ proposed here appropriately incorporates the setup effect and considers the scale effects between the piezocone and pile and hence is more advanced than the resistance factors that is incapable of reflecting the time-dependent pile toe resistance; $\bar{q}_e$ is the average effective cone resistance in the pile toe influence zone, which is in the range of about 4–8 times of pile diameter above and below the pile toe [45]. Here, the average effective cone resistance is utilized here to accommodate the scale effect due to the difference in piezocone and pile diameters.

Similar to the time-dependent pile shaft resistance factor $\alpha_c(t)$, the time-dependent pile toe resistance factor $C_q(t)$ can be also expressed in terms of the degree of consolidation as

$$C_q(t) = C_q(t=0) + \left[C_q(t=\infty) - C_q(t=0)\right]U_{pile}(t) \tag{31}$$

Taking advantage of Eqs. (16) and (31), the time-dependent pile toe resistance factor $C_q(t)$ can be related to the dissipation data from piezocone as follows:

$$C_q(t) = C_q(t=0) + \left[C_q(t=\infty) - C_q(t=0)\right] \left[1 - \frac{\Delta u_{CPTu}\left(D_{pile}^2 t / D_{CPTu}^2\right)}{\Delta u_{CPTu}(t=0)}\right] \quad (32)$$

4.3 Total load carrying capacity

Based on Eqs. (25) and (30), the time-dependent total load carrying capacity, $Q_u(t)$, of a jacked pile in a layered soil can be readily determined as

$$Q_u(t) = F_{su}(t) + F_{qu}(t) = \sum_{i=1}^{n} f_{su,i}(t) A_{s,i} + A_p q_{bu}(t) \quad (33)$$

where $F_{su}(t)$ and $F_{qu}(t)$ are the pile shaft bearing capacity and the pile toe capacity, respectively; $f_{su,i}(t)$ is the time-dependent ultimate shaft resistance in layer i; $A_{s,i}$ is the area of the pile shaft in layer i; and A_p is the cross-sectional area of the pile.

5 Prediction of time-dependent load–displacement behaviour

5.1 Time-dependent load-transfer curves

Generally, pile is designed with sufficient safety factor and the axial load applied on the pile is much smaller than the ultimate load carrying capacity of the pile. In such circumstances, the load–displacement behaviour of the pile becomes the major concern in the design of pile foundations. In this study, the CPTu measurements will be applied to develop the time-dependent nonlinear load-transfer curve for the widely used load-transfer method, while the algorithm of the load-transfer method itself, which can be found from many well-stabilized publications (e.g. [30, 31, 73], will not be discussed in this study.

Currently, there are a variety of load-transfer curves that exist for the analysis of the load–displacement response, such as the elastic perfectly plastic bilinear model [44], the hyperbolic nonlinear model [30, 75], the exponential nonlinear model [65] and the softening nonlinear model [73]. Among these models, the hyperbolic-type and the exponential-type nonlinear models, which can be fully determined by two model parameters, are the most widely used load-transfer curves because of their simplicity and their capability of incorporating the nonlinear soil behaviour. For the hyperbolic-type and the exponential-type load-transfer curves, the two model parameters can be directly or indirectly related to the shear strength and the shear modulus of the soil. Therefore, the model parameters could be possibly determined by the CPTu measurements via the developed shear strength and shear modulus. In this study, the CPTu measurement will be utilized to determine the two model parameters of the exponential-type load-transfer curve. It should be noted that the proposed approach is also applicable to the hyperbolic type and other types of load-transfer curves provided that the model parameters can be determined by the shear strength and the shear modulus of the soil. The function of the time-dependent exponential-type load-transfer curves, as shown in Fig. 6, for pile shaft and pile toe can be given, respectively, as [34, 65]

$$\tau_{s,z}(t) = a_{s,z}(t)\left[1 - e^{-b_{s,z}(t) W_{s,z}}\right] \quad (34)$$

$$q_b(t) = a_b(t)\left(1 - e^{-b_b(t) W_b}\right) \quad (35)$$

where $\tau_{s,z}(t)$ and $W_{s,z}$ are the mobilized shaft shear resistance and the corresponding pile–soil relative displacement at depth z, respectively; $a_{s,z}(t)$ and $b_{s,z}(t)$ are the two time-dependent model parameters of the load-transfer curve for the pile shaft; $q_b(t)$ and W_b are the mobilized resistance and the corresponding displacement at pile toe; and $a_b(t)$ and $b_b(t)$ are the time-dependent model parameters of the load-transfer curve for the pile toe.

5.2 Determination of model parameters

As shown in Fig. 6, the model parameters, $a_{s,z}(t)$ and $a_b(t)$, represent the asymptotic values of the load-transfer curves when the pile–soil relative displacements are sufficient large. Hence, they can be related to the ultimate pile shaft and toe resistance through a failure ratio, respectively, as follows:

$$a_{s,z}(t) = R_f f_{su,z}(t) \quad (36)$$

$$a_b(t) = R_f q_{bu}(t) \quad (37)$$

where R_f is the failure ratio, the value of which is in the range of 0.8–0.95 [16].

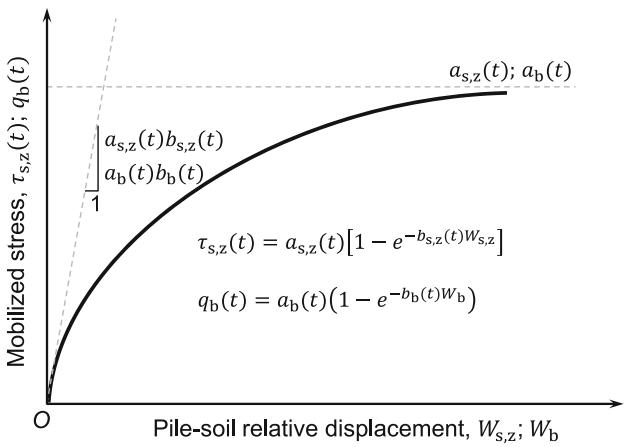

Fig. 6 Exponential type of load-transfer curves for pile shaft and base

Substituting Eqs. (25) and (30) into Eqs. (36) and (37), the model parameters $a_{s,z}(t)$ and $a_b(t)$ can be determined by the CPTu measurements, respectively, as follows:

$$a_{s,z}(t) = R_f \alpha_c(t) q_e \tag{38}$$

$$a_b(t) = R_f C_q(t) \bar{q}_e \tag{39}$$

From Fig. 6, it can be seen that the product of $a_{s,z}(t)$ and $b_{s,z}(t)$ represents the initial tangent stiffness of the load-transfer curve, the value of which is equal to the initial stiffness of the soil column with unit length at the pile–soil interface. Based on Eqs. (16), (20) and (22), the initial stiffness, $K_{0,z}(t)$, can be determined with consideration of the installation effects as follows [32]:

$$K_{0,z}(t) = \begin{cases} \dfrac{2\pi B G_{0,z}}{\ln\left(\dfrac{A - B\ln r_p}{A - B\ln r_m}\right)} & r_y \geq r_m \\ \dfrac{2\pi B G_{0,z}}{\ln\left[\dfrac{A - B\ln r_p}{A - B\ln r_m}\left(\dfrac{r_m}{r_y}\right)^B\right]} & r_y < r_m \end{cases} \tag{40}$$

where r_m $(= 2.5L\chi(1-\nu))$ is the limiting radius, beyond which the shear stress induced by pile loading is negligible; L is the length of the pile; χ is defined as the ratio of soil shear modulus at middle depth of the pile to that at the pile toe; and the coefficients A and B are used to simplify the expression, which are given as

$$A = \left(\frac{\mathrm{OCR}}{2}\right)^{\Lambda} + \frac{1+\nu'}{3(1-\nu')}\left[\frac{3K_0}{2K_0+1} + \frac{1}{\sqrt{3}}\eta_y^* + \left(\frac{\mathrm{OCR}}{2}\right)^{\Lambda}\left(\xi \ln r_p - \frac{\xi}{2} \pm \frac{\sqrt{4M^2 - 3\xi^2}}{6} - 1\right)\right] U_{\mathrm{pile}}(t) \tag{41}$$

$$B = \xi \frac{1+\nu'}{3(1-\nu')}\left(\frac{\mathrm{OCR}}{2}\right)^{\Lambda} U_{\mathrm{pile}}(t) \tag{42}$$

Combining Eqs. (38) and (40) and considering the definition of the product of $a_{s,z}(t)$ and $b_{s,z}(t)$, the model parameter $b_{s,z}(t)$ can be determined by the CPTu measurement as follows:

$$b_{s,z}(t) = \begin{cases} \dfrac{B G_{0,z}}{R_f \alpha_c(t) q_e r_p \ln\left(\dfrac{A - B\ln r_p}{A - B\ln r_m}\right)} & r_y \geq r_m \\ \dfrac{B G_{0,z}}{R_f \alpha_c(t) q_e r_p \ln\left[\dfrac{A - B\ln r_p}{A - B\ln r_m}\left(\dfrac{r_m}{r_y}\right)^B\right]} & r_y < r_m \end{cases} \tag{43}$$

Similarly, the product of $a_b(t)$ and $b_b(t)$ represents the initial stiffness of the pile toe. Following the framework proposed by Randolph and Wroth [48] for analysing the elastic displacement of axially loaded piles, the time-dependent initial stiffness of the pile toe, $K_{0,b}(t)$, can be developed based on Eq. (22) as follows:

$$K_{0,b} = \frac{4\rho_G(t) G_0 r_p}{1-\nu'} \tag{44}$$

From Eqs. (39) and (44) and the definition of the product of $a_b(t)$ and $b_b(t)$, the model parameter $b_b(t)$ can be determined by the CPTu measurements as

$$b_b(t) = \frac{4\rho_G(t) G_0}{\pi r_p C_q(t) \bar{q}_e (1-\nu')} \tag{45}$$

It can be seen from Eqs. (38), (39), (43) and (45) that the time-dependent load-transfer curves for pile shaft and pile toe can be readily determined with the CPTu measurements, and the only additional soil parameters required in the approach are the friction angle and the slope of swelling lines in the e-ln p' plane, which can be obtained from the laboratory tests or empirically estimated based on the practical experience.

Figure 7 shows the flow chart of the procedures of the proposed CPTu method corresponding to the above derivations. It can be seen that the proposed CPTu method

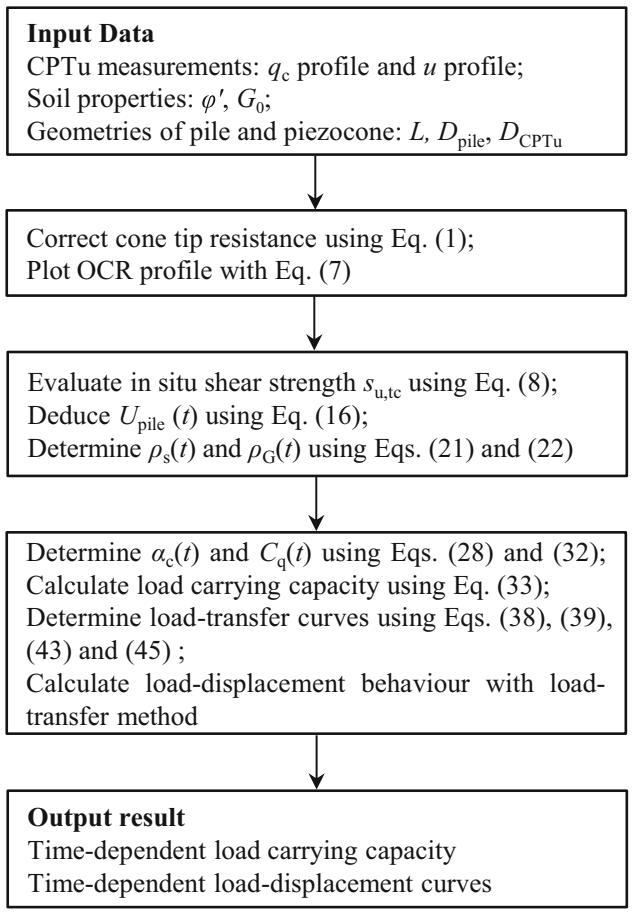

Fig. 7 Flow chart for procedures of proposed method

only requires the CPTu measurements, the friction angle and in situ shear modulus of the soil and the geometry information of the pile and the piezocone as the input data. With these input data, the time-dependent load carrying behaviours of the pile could be easily predicted by the proposed method with the aid of a simple MATLAB code.

6 Centrifuge model tests

To validate of the proposed CPTu approach, centrifuge model tests were designed and conducted in the centrifuge facility at Tongji University, Shanghai, China. The tests include two groups pile loading tests at different times after installation and a piezocone penetration and dissipation test. The dimension of the strong box used in the test is 600 mm × 400 mm × 500 mm in length, width and height, respectively. The designed acceleration level of the tests was 50 g. The scale factors involved in centrifuge model tests are listed in Table 1.

The soil sample used in the tests was the reconstituted Shanghai silty clay. The homogeneous slurry, prepared by stirring the mixture of the clay powder and water in a vacuum tank, was consolidated under the K_0 condition in the strong box at a centrifugal acceleration of 50 g. The consolidation lasted for 10 h, which is equivalent to 35-month consolidation time for the prototype clay sample and is long enough to fully consolidate the soil sample. The loading system, consisting of an electrical motor jack equipped with a step motor to control the loading rate, was installed at the top of the strong box for pile installation and loading tests. Six close-ended hollow aluminium alloy model piles: three with an outer diameter of 12 mm and three with outer diameters of 16 mm, were used in the tests to explore the time-dependent load carrying behaviours of piles with different diameters. The load carrying capacity of the pile was measured by a force transducer, which was mounted at the top of the model pile through threaded caps, as shown in Fig. 8. The piezocone used in the test was the miniature piezocone with an effective length of 300 mm, shaft diameter of 10 mm and apex angle of 60°. The piezocone utilized could simultaneously measure and record the cone tip resistance, pore water pressures at the cone shoulder and the sleeve friction during penetration.

Table 1 Scale factors in centrifuge modelling

Quantity	Scale factor
Length	$1/N$
Gravity	$1/N$
Mass	$1/N^3$
Force	$1/N^2$
Stress	1
Moduli	1
Acceleration	N
Time (consolidation)	$1/N^2$

In the first and second group tests, one model pile was firstly pushed into the soil sample at a constant rate of 90 mm/min under the centrifuge acceleration of 50 g until it reaches the designed embedded depth of 200 mm. Subsequently, the pile loading test was conducted 5 min after installation by pushing the pile down at a relative slow rate of 5 mm/min. After that, the other two piles were installed and pile loading tests were performed successively following the same procedure, but the loading tests were conducted 10 min and 60 min after installation, respectively, to investigate the load carrying behaviours of the pile at different times after installation. In the tests, every pile was tested only once to avoid the repeating loading effect impacting the load carrying behaviours of the pile. During pile loading process, the loads imposed on the pile were recorded by a force transducer, while the displacement of the pile could be deducted from the loading rate and time. It should be noted that in the test the minimum space between the pile and the wall of the strong box was 135 mm and the minimum space between the individual piles was 150 mm, which are larger enough to avoid the boundary effect and the interaction effect between the piles [24].

After the pile loading tests, the CPTu was conducted by pushing the piezocone into the soil sample at a constant rate of 90 mm/min under the acceleration of 50 g (20 mm/

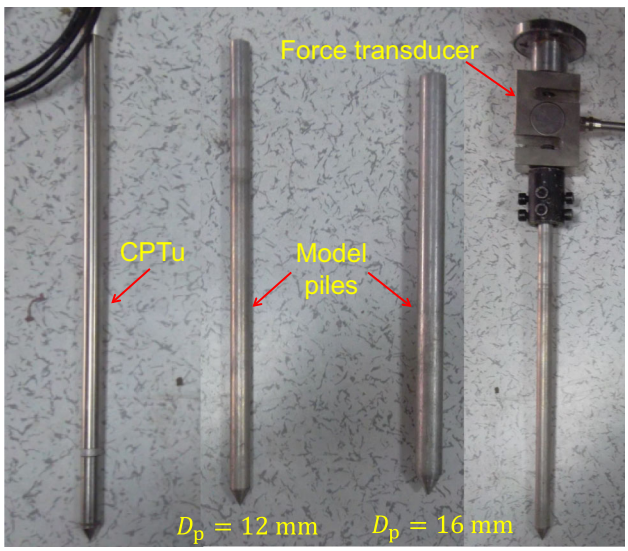

Fig. 8 Picture of model piles and piezocone used in centrifuge model tests

Table 2 Pile shaft capacity, end capacity and total capacity at different times

$D = 0.6$ m					$D = 0.8$ m			
t (days)	F_{su} (kN)	F_{qu} (kN)	Q_u (kN)	F_{su}/Q_u (%)	F_{su} (kN)	F_{qu} (kN)	Q_u (kN)	F_{su}/Q_u (%)
0	125.48	39.03	164.51	76.28	167.31	69.38	236.69	70.69
8.65	239.72	63.78	303.49	78.99	277.75	101.29	379.03	73.28
17.3	274.69	71.36	346.04	79.38	327.86	115.76	443.62	73.91
105	325.50	82.37	407.86	79.81	420.93	142.65	563.59	74.69

s under 1 g condition). When the piezocone reached the prescribed depth of 240 mm, the penetration process halted and the dissipation test was performed until the pore pressure readings decay to the hydrostatic pore water pressure under the acceleration of 50 g. The cone tip resistance q_t and the pore water pressure at the cone shoulder u_2 were continuously recorded in the whole process, which will be utilized to predict the time-dependent load carrying behaviours of the model piles.

Figure 9 shows the plot of the load–displacement curves from the two groups of pile loading tests. The load–displacement curves exhibit apparent time-dependent behaviour after installation. The stiffness of the load–displacement curves increase significantly with the passage of time, which is more pronounced for the piles with lager diameter. It is also observed that all the load–displacement curves show plunging failure, after which the displacement increases significantly but the load increases little. For this type of failure, the load carrying capacity of the pile can be readily considered as the load at the onset of the plunging failure [24]. Hence, the loads corresponding to the plunging failure (Table 2) will be compared with the predictions to validate the proposed method latter in the paper.

Figure 10 shows the profiles of the cone tip resistance q_c and the penetration pore water pressure u_2 at the shoulder of the cone during sounding. It can be seen that both the tip resistance and the pore pressure increase almost linearly with the increase in depth. This indicates that the soil sample is homogeneous as it was prepared by reconsolidation of the homogeneous slurry under the constant centrifuge acceleration.

The measured dissipation data of the excess pore water pressure at the shoulder of the cone are presented in Fig. 11. As shown in the figure, the dissipation curve decreases with elapse of time, and the time required for full dissipation of the excess pore water pressure induced by penetration lasts about 4000 s. At the beginning of the dissipation test, the excess pore water pressure dissipates rapidly, while the dissipation rate decreases significantly with time due to the decrease in the pressure gradient. Dissipation of 90% of the excess pore water pressure lasts about 1400 s; after that, the pore water pressure nearly keeps unchanged and gradually approaches the hydrostatic pore water pressure.

7 Validation of proposed CPTu approach

In this section, the proposed approach is applied to predict the time-dependent load carrying behaviours of the model piles so as to show the application of the proposed CPTu

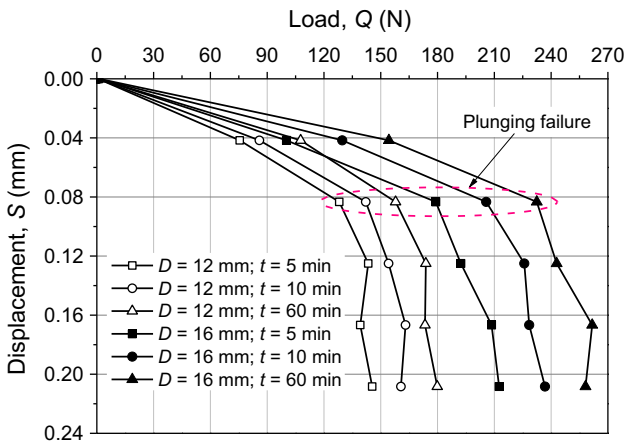

Fig. 9 Load–displacement curves measured from centrifuge model test

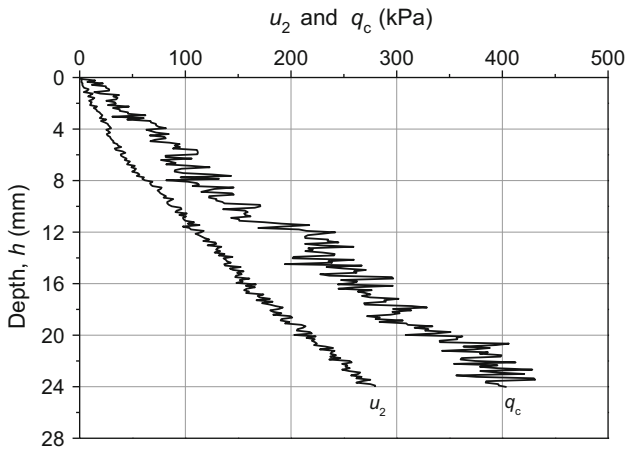

Fig. 10 Profiles of cone tip resistance and pore water pressure with depth

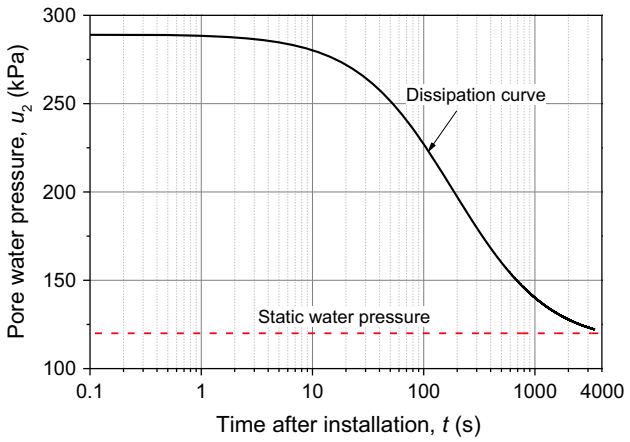

Fig. 11 Dissipation curve of pore water pressure measured from dissipation test

method. For clarity, the interpreted results and the comparisons are displayed in terms of the prototype. According to the scale factors listed in Table 1, the dimensions of the model pile are scaled up by a factor of 0.02, the time for consolidation is scaled up by a factor of 4×10^{-4}, while the stress and strain were scaled up by a factor of 1. The friction angle φ' and the shear modulus G_0, the two additional soil parameters required in the proposed approach, have been determined to be $\varphi' = 31.7^\circ$ and $G_0/p'_0 = 430$, respectively, from the laboratory tests on the soil sample retrieved after the centrifuge tests.

Figure 12 shows the plot of the profiles of the corrected cone resistance q_t, the effective cone resistance q_e, the interpreted shear strength under triaxial condition $s_{u,tc}$ and the interpreted shaft resistance f_{su} with depth. Based on the profile of the cone tip resistance shown in Fig. 12, the profile of OCR along the depth can be obtained by making use of Eq. (7). The resulting profile of the OCR is shown in

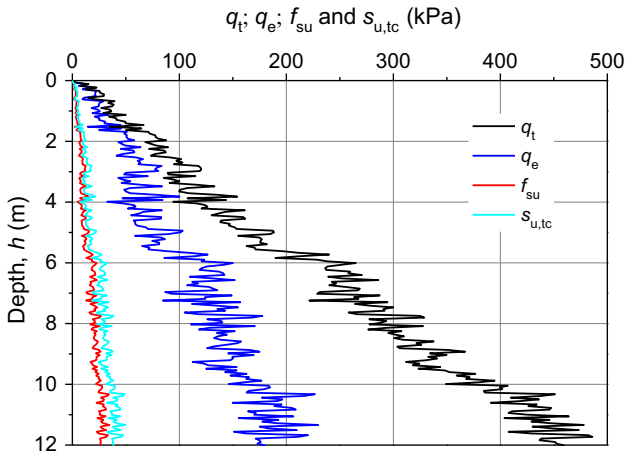

Fig. 12 Profiles of corrected cone resistance, effective cone resistance, interpreted shear strength under triaxial condition and shaft resistance with depth

Fig. 13. It can be observed that the soil sample is a little overconsolidated with OCR in the order of 1.1. This is because the centrifuge facility was stopped after each pile loading test to install the model pile on the electrical motor for the next pile installation and loading test. Although the duration of unloading periods lasted just about 10 min each time, which was a relative short time period compared with the spinning time, the soil sample was inevitably unloaded during this process. Hence, the OCR measured from the CPTu test conducted after pile loading test showed that the soil sample is a little overconsolidated with OCR on the order of 1.1.

From the pore water pressure dissipation curve measured from the centrifuge model test shown in Fig. 11, the corresponding dissipation curve in terms of prototype and the curves of degree of consolidation for the soil adjacent to the piezocone and two types of model pile can be deduced from the scale factors listed in Table 1 and Eqs. (15) and (16), which are plotted in Fig. 14. Following the empirical formula, $K_0 = \mathrm{OCR}^{\sin\varphi'}(1 - \sin\varphi')$, proposed by Mayne and Kulhawy [41], the coefficient of earth pressure at rest, K_0, of the soil sample can be determined as 0.5. Based on the deduced degree of consolidation shown in Fig. 14 and the interpreted soil parameters shown in Figs. 12 and 13, the time-dependent shaft resistance factor $\alpha_c(t)$ and the pile base resistance factor $C_q(t)$ can be readily determined by Eqs. (28) and (32), respectively. The theoretically derived unit shaft resistances along pile shaft at various maturities of the pile loading test are plotted in Fig. 15, based on which the time-dependent load carrying capacity of the pile can be determined by Eq. (33). Figure 16 shows the comparisons of the predicted and the measured time-dependent load carrying capacities of the model piles. Since the dissipation test lasted 100 days, the predicted maximum time span for the model pile with a diameter of 0.6 m is 144 days and for the pile with a

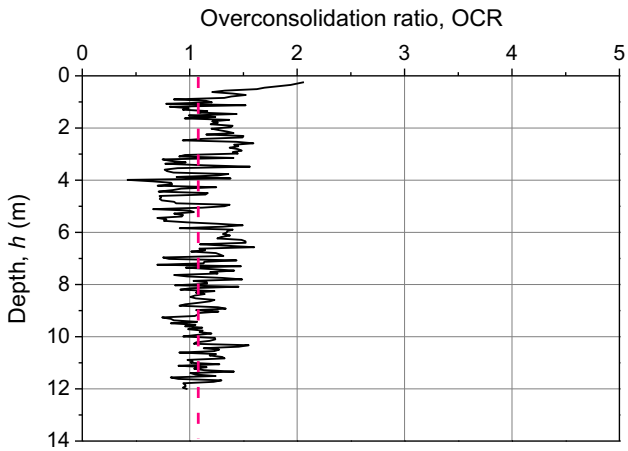

Fig. 13 Profile of interpreted overconsolidation ratio with depth

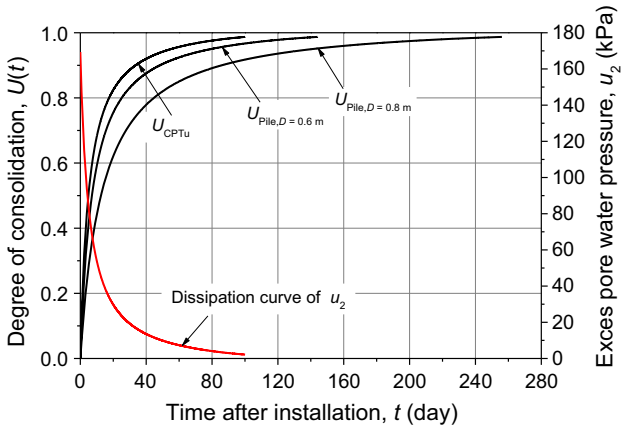

Fig. 14 Degree of consolidation deduced from excess pore water pressure dissipation curve

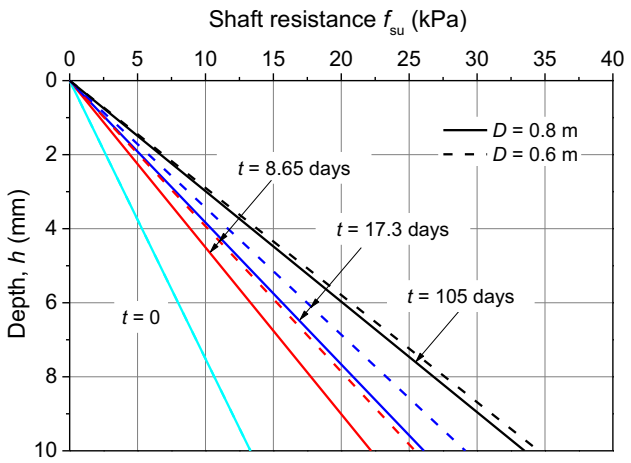

Fig. 15 Theoretically derived unit shaft resistances along pile shaft at different times after pile installation

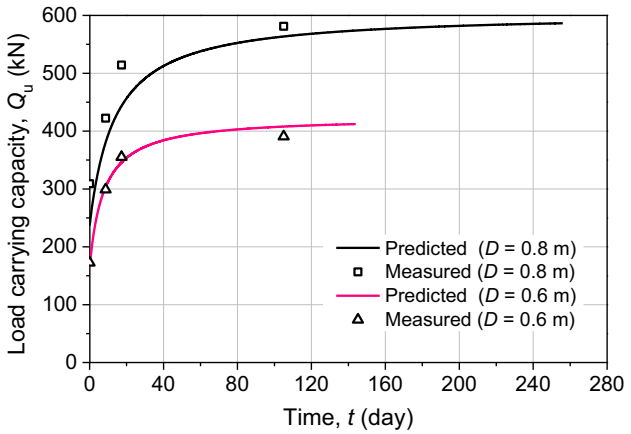

Fig. 16 Comparison between predicted and measured load carrying capacities

diameter of 0.6 m is 256 days. As shown in the figure, the predictions agree well with the results measured from the centrifuge model tests, which indicates the proposed approach is capable of providing reasonable predictions for the time-dependent load carrying capacity of the pile based on the CPTu measurements. It is also interesting to find that the pile with lager diameter exhibits larger load carrying capacity but requires more time to reach the final limit state. This means that it will cost more time to determine the long-term load carrying capacity for the large diameter piles from the pile loading test, which indirectly highlights the significance and advantage of the proposed approach.

It should be noted that the diameter of the miniature piezocone used in the centrifuge model test is 10 mm, which corresponds to a prototype piezocone with a diameter of 0.5 m. Hence, the piezocone dissipation test lasts more than 100 days in this study. For a standard piezocone with a diameter of 3.6 cm in practice, it can be deduced based on Eq. (7) that it only requires 0.5 day for full dissipation of the excess pore water. Hence, the proposed approach could provide a time-efficient and feasible way to predict the time-dependent load carrying behaviours of the jacked pile in practice, especially for the pile with larger diameters.

Based on the developed load-transfer curves, the time-dependent load–displacement behaviours of the model piles can be predicted by the load-transfer method. Figure 17 shows the predicted and the measured load–displacement curves for the model piles at different times after installation. As shown in the figure, the predicted curves match well with the measured curves, which again demonstrate the validity of the proposed CPTu method. Corresponding to the dissipation curve shown in Fig. 14, the stiffness and the capacity of the pile shown in Fig. 17 increase rapidly at the beginning of consolidation, while the rate decreases with passage of time. This sufficiently manifests that the increase in the mean effective stress due to consolidation is the primary cause for the setup of the jacked pile in clayey soils.

The above comparisons indicate that the proposed CPTu approach is capable of yielding reasonable predictions for the time-dependent load carrying behaviours of the model piles by making use of CPTu measurements. However, since the diameter of the miniature piezocone employed in the centrifuge model test is close to the diameters of the model piles, the scale effects between the piezocone and the pile may not be well reflected by the centrifuge model test. Moreover, although the discrepancy of the displacements to mobilize the shaft and toe ultimate resistances in the centrifuge model tests is not pronounced as the diameter of the model pile used in the centrifuge model test is relatively small, the discrepancy in required displacements to develop shaft and toe ultimate resistances has a pronounced effect on the total bearing capacity for the actual piles with a larger diameter. Furthermore, due to lack of the

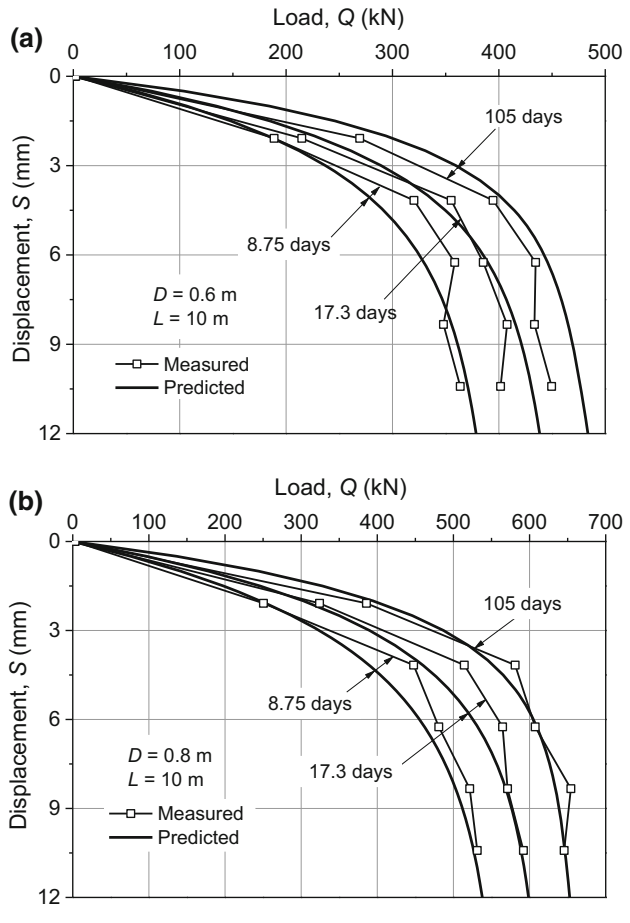

Fig. 17 Comparison between predicted and measured load–settlement behaviours of model piles at different times after installation: **a** $D_{\text{pile}} = 0.6\,\text{m}$; **b** $D_{\text{pile}} = 0.8\,\text{m}$

field data, the proposed CPTu method is only validated by the centrifuge model tests conducted in the homogeneous normally consolidated clay. Therefore, the proposed CPTu method still needs further validation and calibration with field data that cover a wide range of pile diameters and soil conditions before it is applied in practical engineering.

8 Conclusions

In this paper, a feasible CPTu method is developed to predict the time-dependent load carrying behaviours of jacked piles. The corrected cone resistance, considering the unequal area of the cone rod and the cone, is used to determine the shear strength and the OCR of the soil for the proposed approach. Based on the similarity between the pile and the piezocone, the time-dependent pile shaft and base resistance factors as well as the time-dependent load-transfer curves are developed by making use of the cone tip resistance, the pore water pressure during sounding and the subsequent pore water pressure dissipation data of CPTu. The three-dimensional strength and anisotropic initial stress of the soil, the pile installation effects and the scale effects between the pile and the piezocone, all of which are of great significance to determine the load carrying behaviours of the jacked pile, are properly considered in the proposed approach. The only additional soil parameters required in the approach are the friction angle and the in situ shear modulus, which can be easily obtained from the laboratory tests or empirically assumed based on the practical experience.

Centrifuge model tests, including two groups pile loading tests at different times after pile installation and a piezocone penetration and dissipation test, were conducted for validation of the proposed CPTu method. The proposed approach is then applied to predict the time-dependent load carrying behaviours of the model piles using the CPTu measurements so as to illustrate the application and validity of the proposed CPTu method. The results show that the proposed approach is capable of yielding reasonable predictions for the time-dependent load carrying behaviours of jacked piles. The proposed provides a time-efficient and feasible way to predict the time-dependent load carrying behaviours of the jacked pile in clay, which not only greatly saves the time of conducting time-consuming pile loading tests, but also effectively avoids solving the complex partial differential equations involved in consolidation analysis. However, due to lack of field tests conducted specifically to investigate the relation between the CPTu dissipation data and the time-dependent load carrying capacity of the jacked piles, the proposed approach is only verified by the centrifuge model tests conducted by the authors. The miniature piezocone used in the centrifuge model test corresponds to a prototype piezocone with a diameter of 0.5 m, which is much larger than the diameter of the standard piezocone with a diameter of 3.6 cm in practice. Moreover, the diameters of the two type model piles in terms of the prototype are 0.6 m and 0.8 m, respectively, which cover a limited range of pile diameter and are close to the diameter of the piezocone. Hence, the scale effects between the pile and the piezocone and the discrepancy in required displacements to develop shaft and toe ultimate resistances were not well reflected by the centrifuge model tests. Therefore, filed tests that use the standard piezocone and cover a wide range of pile diameters and soil conditions are expected to be conducted for further validation and calibration of the proposed CPTu method before it is used in practical engineering. It should also be declared that the proposed CPTu method is developed for jacked piles, which may not be applicable to other types of displacement piles as the installation effects and time-dependent load carrying behaviour of other type piles are more or less different from those of jacked piles.

Acknowledgements The authors are grateful for the financial support provided by the National Natural Science Foundation of China (Grant No. 41772290) for this research work.

References

1. Abufarsakh MY, Titi HH (2004) Assessment of direct cone penetration test methods for predicting the ultimate capacity of friction driven piles. J Geotech Geoenviron Eng 130(9):935–944
2. Abufarsakh MY, Rosti F, Souri A (2015) Evaluating pile installation and subsequent thixotropic and consolidation effects on setup by numerical simulation for full-scale pile load tests. Can Geotech J 52(11):1734–1746
3. Agaiby S, Mayne PW (2018) Interpretation of piezocone penetration and dissipation tests in sensitive Leda clay at Gloucester test site. Can Geotech J 55(12):1781–1794
4. Augustesen AH (2006) The effects of time on soil behaviour and pile capacity. Doctoral dissertation, Aalborg University, Department of Civil Engineering
5. Baligh MM (1985) Strain path method. J Geotech Eng 111(9):1108–1136
6. Basu P, Prezzi M, Salgado R, Chakraborty T (2014) Shaft resistance and setup factors for piles jacked in clay. J Geotech Geoenviron Eng 140(3):04013026
7. Bond AJ (1989) Behaviour of displacement piles in overconsolidated clays. Ph.D. thesis, Imperial College London, London, UK
8. Bullock PJ, Schmertmann JH, McVay MC, Townsend FC (2005) Side shear setup. I: test piles driven in Florida. J Geotech Geoenviron Eng 131(3):292–300
9. Burns SE, Mayne PW (1995) Coefficient of consolidation (c_h) from type 2 piezocone dissipation in overconsolidated clays. In: Proceedings, International Symposium on Cone Penetration Testing (CPT '95), Linkøping, Sweden, vol 2, pp 137–142
10. Burns SE, Mayne PW (1998) Monotonic and dilatory pore-pressure decay during piezocone tests in clay. Can Geotech J 35(6):1063–1073
11. Cai GJ, Liu SY, Tong LY, Du GY (2009) Assessment of direct CPT and CPTU methods for predicting the ultimate bearing capacity of single piles. Eng Geol 104(3–4):211–222
12. Cao LF, Teh CI, Chang MF (2001) Undrained cavity expansion in modified Cam clay I: theoretical analysis. Géotechnique 51(4):323–334
13. Chang MF, Teh CI, Cao LF (2001) Undrained cavity expansion in modified Cam clay II: application to the interpretation of the piezocone test. Géotechnique 51(4):335–350
14. Chen JJ, Zhang LY (2013) Effect of spatial correlation of cone tip resistance on the bearing capacity of piles. J Geotech Geoenviron Eng 139(3):494–500
15. Chow FC (1997) Investigations into the behaviour of displacement piles for offshore foundations. Imperial College London, London
16. Clough GW, Duncan JM (1971) Finite element analyses of retaining wall behavior. J Soil Mech Found Div ASCE 97(12):1657–1673
17. Dafalias YF (1987) An anisotropic critical state clay plasticity model. In: Proceedings of the constitutive laws for engineering materials: theory and applications, Tucson, pp 513–521
18. De Chaunac H, Holeyman A (2018) Numerical analysis of the set-up around the shaft of a closed-ended pile driven in clay. Géotechnique 68(4):332–344
19. De Kuiter J, Beringen FL (1979) Pile foundations for large North Sea structures. Mar Georesour Geotechnol 3(3):267–314
20. Doherty P, Gavin K (2011) The shaft capacity of displacement piles in clay: a state of the art review. Geotech Geol Eng 29(4):389–410
21. Eslami A, Fellenius BH (1997) Pile capacity by direct CPT and CPTu methods applied to 102 case histories. Can Geotech J 34(6):886–904
22. Fateh AMA, Eslami A, Fahimifar A (2017) Direct CPT and CPTu methods for determining bearing capacity of helical piles. Mar Georesour Geotechnol 35(2):193–207
23. Guo WD (2000) Visco-elastic consolidation subsequent to pile installation. Comput Geotech 26(2):113–144
24. Hesham M, Naggar E, Sakr M (2000) Evaluation of axial performance of tapered piles from centrifuge tests. Can Geotech J 37(6):1295–1308
25. Hu Z, McVay M, Bloomquist D, Horhota D, Lai P (2012) New ultimate pile capacity prediction method based on cone penetration test (CPT). Can Geotech J 49(8):961–967
26. Huang W, Sheng D, Sloan SW, Yu HS (2004) Finite element analysis of cone penetration in cohesionless soil. Comput Geotech 31(7):517–528
27. Khanmohammadi M, Fakharian K (2017) Numerical modelling of pile installation and set-up effects on pile shaft capacity. Int J Geotech Eng 13:484–498
28. Khanmohammadi M, Fakharian K (2018) Numerical simulation of soil stress state variations due to mini-pile penetration in clay. Int J Civ Eng 16(4):409–419
29. Kraft LM, Focht JA, Amerasinghe SF (1981) Friction capacity of piles driven into clay. J Geotech Geoenviron Eng 107(GT 11):1521–1541
30. Kraft LM, Ray RP, Kakaaki T (1981) Theoretical t–z curves. J Geotech Eng Div 107(11):1543–1561
31. Lee KM, Xiao ZR (2001) A simplified nonlinear approach for pile group settlement analysis in multilayered soils. Can Geotech J 38(5):1063–1080
32. Li L, Li JP, Sun DA (2016) Anisotropically elasto-plastic solution to undrained cylindrical cavity expansion in K_0-consolidated clay. Comput Geotech 73:83–90
33. Li L, Li JP, Sun DA, Gong WB (2017) Analysis of time-dependent bearing capacity of a driven pile in clayey soils by total stress method. Int J Geomech 17(7):04016156
34. Li L, Li JP, Sun DA, Gong WB (2017) Semi-analytical approach for time-dependent load–settlement response of a jacked pile in clay strata. Can Geotech J 54(12):1682–1692
35. Lunne T, Eidsmoen T, Gillespie D, Howland JD (1986) Laboratory and field evaluation of cone penetrometers. In: Proceedings of the ASCE specialty conference on use of in situ tests in geotechnical engineering, Blacksburg, Virginia, pp 714–729
36. Matsuoka H (1976) On the significance of the "spatial mobilized plane". Soils Found 16(1):91–100
37. Matsuoka H, Sun DA (2006) The SMP concept-based 3D constitutive models for geomaterials. Taylor and Francis, Leiden
38. Matsuoka H, Yao Y, Sun D (1999) The Cam-clay models revised by the SMP criterion. Soils Found 39(1):81–95
39. Mayne PW (1991) Determination of OCR in clays by piezocone tests using cavity expansion and critical state concepts. Soils Found 31(2):65–76
40. Mayne PW, Holtz RD (1988) Profiling stress history from piezocone soundings. Soils Found 28(1):16–28
41. Mayne PW, Kulhawy FH (1982) K_0-OCR relationships in soil. J Geotech Eng Div 108(6):851–872
42. Mayne PW, Niazi FS (2009) Evaluating axial elastic pile response from cone penetration tests (The 2009 Michael W. O'Neill Lecture). DFI J J Deep Found Inst 3(1):3–12
43. Mayne PW, Elhakim A (2002) Axial pile response evaluation by geophysical piezocone tests. In: Proceedings of the 9th

international conference on piling and deep foundations, DFI, Nice, Presses de l'ecole nationale des Ponts et chaussees, pp 543–550
44. Motta E (1994) Approximate elastic-plastic solution for axially loaded piles. J Geotech Eng 120(9):1616–1624
45. Niazi FS, Mayne PW (2013) Cone penetration test based direct methods for evaluating static axial capacity of single piles. Geotech Geol Eng 31(4):979–1009
46. Niazi FS, Mayne PW (2016) CPTu-based enhanced UniCone method for pile capacity. Eng Geol 212:21–34
47. Randolph MF (2003) Science and empiricism in pile foundation design. Géotechnique 53(10):847–876
48. Randolph MF, Wroth CP (1979) An analysis of the vertical deformation of pile groups. Géotechnique 29(4):423–439
49. Randolph MF, Wroth CP (1979) An analytical solution for the consolidation around a driven pile. Int J Numer Anal Methods Geomech 3(3):217–229
50. Randolph MF, Wroth CP (1981) Application of the failure state in undrained simple shear to the shaft capacity of driven piles. Géotechnique 31(1):143–157
51. Randolph MF, Carter JP, Wroth CP (1979) Driven piles in clay-the effects of installation and subsequent consolidation. Géotechnique 29(4):361–393
52. Robertson PK, Woeller DJ, Gillespie D (1990) Evaluation of excess pore pressures and drainage conditions around driven piles using the cone penetration test with pore pressure measurements. Can Geotech J 27(2):249–254
53. Roy M, Blanchet R, Tavenas F, Rochelle PL (1981) Behaviour of a sensitive clay during pile driving. Can Geotech J 18(1):67–85
54. Roy M, Tremblay M, Tavenas F, Rochelle PL (1982) Development of pore pressures in quasi-static penetration tests in sensitive clay. Can Geotech J 19(2):124–138
55. Saldivar EE, Jardine RJ (2005) Application of an effective stress design method to concrete piles driven in Mexico City clay. Can Geotech J 42(6):1495–1508
56. Samson L, Authier J (1986) Change in pile capacity with time: case histories. Can Geotech J 23(2):174–180
57. Schneider JA, Xu X, Lehane B (2008) Database assessment of CPT-based design methods for axial capacity of driven piles in siliceous sands. J Geotech Geoenviron Eng 134(9):1227–1244
58. Skov R, Denver H (1988) Time dependence of bearing capacity of piles. In: Fellenius BH (ed) Proceedings of 3rd international conference on the application of stress-wave theory to piles. BiTech, Ottawa, pp 879–888
59. Sully JP, Robertson PK, Campanella RG, Woeller DJ (1999) An approach to evaluation of field CPTU dissipation data in over-consolidated fine-grained soils. Can Geotech J 36(2):369–381
60. Sun DA, Matsuoka H, Yao YP, Ishii H (2004) An anisotropic hardening elastoplastic model for clays and sands and its application to FE analysis. Comput Geotech 31(1):37–46
61. Suzuki Y, Lehane BM (2015) Analysis of CPT end resistance at variable penetration rates using the spherical cavity expansion method in normally consolidated soils. Comput Geotech 69:141–152
62. Teh CI, Houlsby GT (1991) Analytical study of the cone penetration test in clay. Géotechnique 41(1):17–34
63. Torstensson BA (1977) The pore pressure probe. Geoteknikkdagen, Oslo, Paper 34, pp 34.1–34.15
64. Vardanega PJ, Williamson MG, Bolton MD (2012) Bored pile design in stiff clay II: mechanisms and uncertainty. Proc Inst Civ Eng Geotech Eng 165(4):233–246
65. Wang ZJ, Xie XY, Wang JC (2012) A new nonlinear method for vertical settlement prediction of a single pile and pile groups in layered soils. Comput Geotech 45:118–126
66. Wardle IF, Price G, Freeman J (1992) Effect of time and maintained load on the ultimate capacity of pile in stiff clay. Piling: European Practice and Worldwide Trends: Proceedings of the Conference Organized by the ICE, London, pp 92–99
67. Wheeler SJ, Naatanen A, Karstunen M, Lojander M (2003) An anisotropic elastoplastic model for soft clays. Can Geotech J 40(2):403–418
68. Wood DM (1990) Soil behaviour and critical state soil mechanics. Cambridge University Press, Cambridge
69. Xu X, Schneider JA, Lehane B (2008) Cone penetration test (CPT) methods for end-bearing assessment of open- and closed-ended driven piles in siliceous sand. Can Geotech J 45(8):1130–1141
70. Ye WM, Huang Y, Tang YQ, Lu PJ (2000) Time-effect of bearing capacity of driven pile in saturated soil. Rock Soil Mech 21(4):367–369
71. Yu HS (2000) Cavity expansion methods in geomechanics. Kluwer Academic Publishers, Dordrecht
72. Zhang LY, Chen JJ (2012) Effect of spatial correlation of SPT data on bearing capacity of driven piles in sand. Can Geotech J 49(4):394–402
73. Zhang QQ, Zhang ZM (2012) A simplified nonlinear approach for single pile settlement analysis. Can Geotech J 49(11):1256–1266
74. Zheng JJ, Lu YE, Yin JH, Guo J (2010) Radial consolidation with variable compressibility and permeability following pile installation. Comput Geotech 37(3):408–412
75. Zhu H, Chang MF (2002) Load transfer curves along bored piles considering modulus degradation. J Geotech Geoenviron Eng 128:764–774